Atmos. Chem. Phys., 13, 4941–4961, 2013
www.atmos-chem-phys.net/13/4941/2013/
doi:10.5194/acp-13-4941-2013

Atmospheric Chemistry and Physics Open Access

CO_2 dispersion modelling over Paris region within the CO_2-MEGAPARIS project

C. Lac[1], R. P. Donnelly[1], V. Masson[1], S. Pal[2,3], S. Riette[1], S. Donier[1], S. Queguiner[1], G. Tanguy[1], L. Ammoura[2], and I. Xueref-Remy[2]

[1]CNRM-GAME (CNRS-Meteo-France), UMR3589, Toulouse, France
[2]Laboratoire des Sciences du Climat et de l'Environnement (LSCE), IPSL-UVSQ-CNRS-CEA, Orme des Merisiers, Gif-Sur-Yvette, France
[3]Department of Environmental Sciences, University of Virginia, Charlottesville, Virginia, USA

Correspondence to: C. Lac (christine.lac@meteo.fr)

Received: 11 September 2012 – Published in Atmos. Chem. Phys. Discuss.: 25 October 2012
Revised: 23 March 2013 – Accepted: 3 April 2013 – Published: 14 May 2013

Abstract. Accurate simulation of the spatial and temporal variability of tracer mixing ratios over urban areas is a challenging and interesting task needed to be performed in order to utilise CO_2 measurements in an atmospheric inverse framework and to better estimate regional CO_2 fluxes. This study investigates the ability of a high-resolution model to simulate meteorological and CO_2 fields around Paris agglomeration during the March field campaign of the CO_2-MEGAPARIS project. The mesoscale atmospheric model Meso-NH, running at 2 km horizontal resolution, is coupled with the Town Energy Balance (TEB) urban canopy scheme and with the Interactions between Soil, Biosphere and Atmosphere CO_2-reactive (ISBA-A-gs) surface scheme, allowing a full interaction of CO_2 modelling between the surface and the atmosphere. Statistical scores show a good representation of the urban heat island (UHI) with stronger urban–rural contrasts on temperature at night than during the day by up to 7 °C. Boundary layer heights (BLH) have been evaluated on urban, suburban and rural sites during the campaign, and also on a suburban site over 1 yr. The diurnal cycles of the BLH are well captured, especially the onset time of the BLH increase and its growth rate in the morning, which are essential for tall tower CO_2 observatories. The main discrepancy is a small negative bias over urban and suburban sites during nighttime (respectively 45 m and 5 m), leading to a few overestimations of nocturnal CO_2 mixing ratios at suburban sites and a bias of +5 ppm. The diurnal CO_2 cycle is generally well captured for all the sites. At the Eiffel tower, the observed spikes of CO_2 maxima occur every morning exactly at the time at which the atmospheric boundary layer (ABL) growth reaches the measurement height. At suburban ground stations, CO_2 measurements exhibit maxima at the beginning and at the end of each night, when the ABL is fully contracted, with a strong spatio-temporal variability. A sensitivity test without urban parameterisation removes the UHI and underpredicts nighttime BLH over urban and suburban sites, leading to large overestimation of nocturnal CO_2 mixing ratio at the suburban sites (bias of +17 ppm). The agreement between observation and prediction for BLH and CO_2 concentrations and urban–rural increments, both day and night, demonstrates the potential of using the urban mesoscale system in the context of inverse modelling

1 Introduction

It has been widely reported that atmospheric CO_2 concentration has increased by more than 30 % since the pre-industrial era mainly due to human activities and this increase is very likely at the root of the observed temperature rise of 0.6 °C over the last century (Forster et al., 2007). Although we have good estimates of the CO_2 fluxes on a global basis, and have a relatively well-established observation network to detect the large-scale trends, regional information (10–500 km) is needed if society is ever to manage or verify carbon emissions (Dolman et al., 2006). We must improve our understanding of regional variations in sources and sinks of CO_2 to identify possible sequestration or emission management

options. It is necessary to discriminate between the anthropogenic and biospheric sources which overlap very strongly in European countries. In this context, the project CO_2-MEGAPARIS aims at the quantification of the CO_2 emissions of the megacity Paris and consequently the simulation and assessment of the anthropogenic CO_2 plume over the Ile-de-France province (corresponding to the Paris administrative region) (Xueref-Remy et al., 2012). Indeed, with 12 million of inhabitants, Paris is the third largest megacity of Europe (after London and Moscow), and is estimated to emit about 14 % of national emissions. Moreover, it is an ideal test location due to its relatively well defined boundaries and the lack of other major CO_2 emitters in its immediate vicinity. The former experiment ESQUIF (Vautard et al., 2003) gave a fair understanding of the atmospheric dynamics in this area and the impact on air quality.

The quantification of continental sources and sinks of CO_2 can be improved by regional inversion (the so-called top-down method). In this approach, the variability in atmospheric CO_2 concentrations are observed to better understand the causes of variability in the source–sink distribution by inverting the atmospheric transport. Recent urban CO_2 studies have been pursued with different objectives: for instance, Kort et al. (2012) quantified the urban CO_2 dome over Los Angeles and Mumbai using satellite data, Gurney et al. (2012) aimed the quantification of CO_2 emissions at Indianapolis, and Strong et al. (2011) studied urban CO_2 cycles within Salt Lake Valley. A number of studies have used inverse modelling tools at global and regional scales (Enting, 1993; Rödenbeck et al., 2003; Gurney et al., 2002; Lauvaux et al., 2008, 2009) together with global networks of observations which also recently include tall tower observatories. But the scarcity of concentration measurements and errors in simulating atmospheric transport can introduce large uncertainties. Furthermore, the spread in fluxes induced by transport model differences was found to be almost as large as the uncertainties arising from the lack of adequate observations (Gurney et al., 2002). Using high-resolution atmospheric models to retrieve CO_2 sources and sinks at the regional scale represents major progress, as shown by the model intercomparison study over Europe led by Geels et al. (2007).

The major uncertainties in CO_2 modelling are related to model errors in horizontal wind (Lin and Gerbig, 2005) and vertical transport within the atmospheric boundary layer (ABL) (Gerbig et al., 2008; Kretschmer et al., 2012). The boundary layer height (BLH) is a key variable in modelling atmospheric CO_2 since surface fluxes are mixed up to this height ("first order" approximation), causing the atmospheric CO_2 concentration to be underestimated when the BLH is overestimated, and vice versa, assuming a constant surface source. Geels et al. (2007) showed that in inversion CO_2 studies at low-altitude sites, only the afternoon values of concentrations can be represented sufficiently well and are therefore more appropriate for constraining large-scale sources and sinks in combination with transport models as the stable boundary conditions are highly difficult to represent by the meteorological models (Seibert et al., 2000). Therefore, inversion studies usually tend to impose less statistical weighting (larger uncertainty) or implement temporal data filtering (e.g. selection of afternoon data). Lauvaux et al. (2008) also found that improving the transport simulation for nocturnal CO_2 concentrations at tower sites would lead to large error reduction in CO_2 inversions. In this context a correct representation of the ABL during the night and the morning is challenging.

Also during daytime, Sarrat et al. (2007b), in an intercomparison study of five mesoscale models, showed that BLHs between models revealed considerable discrepancies. The BLH can also be affected by entrainment from overshooting thermals that is often underestimated in mesoscale meteorological models (McGrath-Spangler and Denning, 2010). De Arellano et al. (2004) have shown that the CO_2 concentration in the ABL is reduced much more effectively by the ventilation with entrained air than by CO_2 uptake by the vegetation, especially in the morning hours during the rapid growth of ABL in a rural site in the Netherlands.

Detailed validations of high-resolution forward models using networks of atmospheric measurements are therefore needed to assess how well the transport and variability of atmospheric tracers are represented. A number of studies using high-resolution models showed substantial improvements in simulating atmospheric CO_2 concentrations under various mesoscale flow conditions (Sarrat et al., 2007a; Ahmadov et al., 2009; Perez-Landa et al., 2007). In this context, urban areas are challenging to represent for CO_2 inversion studies: first, emissions are very heterogeneous, and second, BLH is also spatially variable. Angevine et al. (2003) pointed out the important implications of urban–rural contrasts for air quality. However, the nocturnal boundary layer (NBL) is mixed compared to the rural one. If the urban effects are well represented, this can limit the errors of the model generally associated to the stable conditions. The challenge is here to be able to simulate all the urban effects with an appropriate urban model. The performance of urban parameterisations are therefore crucial in simulating the urban boundary layer (UBL) (Lemonsu et al., 2006; Lee et al., 2008).

This work, as part of the CO_2-MEGAPARIS project, uses a high-resolution modelling approach with the Meso-NH model to investigate the variability of CO_2 concentration as well as BLH over Paris agglomeration. During the CO_2-MEGAPARIS campaign from 21–26 March 2011, anticyclonic weather conditions prevailed (clear sky, moderate temperatures and light winds). Pal et al. (2012) already investigated in detail the spatio-temporal variability of the observed BLH without including CO_2 measurements, and they focussed mainly on the first 4 days of the campaign to asses the impact of the urban heat island (UHI) on the boundary layer circulations.

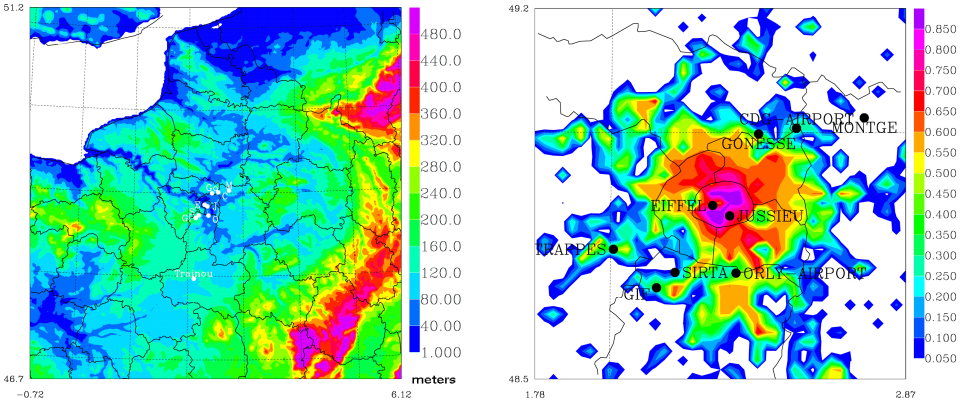

(a) **(b)**

Fig. 1. (a): Domain of simulation with orography (in m a.s.l.). **(b)**: Zoomed-in view on Ile-de-France province with urban fraction. The observational stations (Montge, Gonesse, Eiffel, Jussieu, Trappes, SIRTA, Gif) and airports (CDG and Orly) are labelled on both panels.

The main goals of our study are (1) to test the ability of high-resolution models to represent the spatial and temporal variability of BLH and CO_2 over urban and suburban areas, (2) to evaluate the dynamical effect of urban–rural contrasts on the atmospheric CO_2 field, and (3) to assess the possibility of using these modelling tools in future inversion studies. This paper begins by providing an outline of the modelling strategy and the CO_2-MEGAPARIS dataset, including a description of the specifics of the model setup and the experimental domain (Sects. 2 and 3). This is followed by a validation and discussion of the meteorological predictions against observational data (Sect. 4). The ability of the mesoscale modelling system to reproduce the variability of CO_2 concentration is then examined in urban, suburban and rural sites (Sect. 5). Impact studies of urban surface parameterisation and anthropogenic emissions are led to help in analysing CO_2 emissions and dilution. A summary and a discussion on dominant uncertainties in inverse modelling of CO_2 fluxes follow in Sect. 6.

2 Brief presentation of the CO_2-MEGAPARIS March campaign

The CO_2-MEGAPARIS March experiment field served as a testbed for the project (see http://co2-megaparis.lsce.ipsl.fr), which started on 21 March and ended on 26 March 2011. The meteorological network (described in Pal et al., 2012) was constituted of 3 vertically pointing aerosols lidars and a ceilometer observing quasi-continuous evolution of the BLH operating at the Jussieu (hereafter JUSS) campus in the centre of Paris (Fig. 1b), at the SIRTA observatory representative of a suburban site and located at about 20 km south of Paris, and at Trainou (hereafter TRN) located at a distance of around 100 km to the south of Paris , which is used as a rural background reference site (Fig. 1a). Additionally, radiosounding measurements with a frequency of twice a day (00:00 and 12:00 UTC) were performed at the French operational station Trappes (hereafter TRAP) located in the western suburb of Paris (15 km west of SIRTA). Also, the French operational meteorological surface network includes 270 stations on the simulation domain to evaluate temperature and relative humidity at 2 m and wind fields at 10 m (Fig. 2). The CO_2 monitoring network includes ground CO_2 mixing ratio measurements at the following sites: Gif-sur-Yvette (GIF) located 30 km to the south-west of Paris and 8 km west of Orly Airport; at Gonesse (GON) on the north-east of Paris, 3 km west of Paris-CDG airport; at Montge-en-Goelle (MON), a rural station located 10 km east of Paris-CDG airport; and also at the rural site of TRN (only for 21 March). Additionally, CO_2 mixing ratio measurements were carried out on at the top of the Eiffel tower (310 m, EIF). The CO_2 monitoring stations at GIF and TRN are part of the ICOS infrastructure (http://www.icos-infrastructure.eu/), while the EIF, GON and MON instrumentations were deployed in 2010 within the CO_2-MEGAPARIS project (http://co2-megaparis.lsce.ipsl.fr) and integrated into AIRPARIF network infrastructures. In each station, a ring-down cavity analyser from PICARRO model G1301 was deployed. In the 3 CO_2-MEGAPARIS stations, the observations were made wet and a correction on water vapour was applied using the dedicated Picarro analyser software. All observations were calibrated against the NOAA X2007 scale. Each station was equipped with a calibration and target gas tanks unit owning specific peculiarities. Concerning the GIF and TRN stations, as part of the ICOS infrastructure, an automated gas chromatographic system (HP-6890) was operated for CO_2 measurements of ambient air (Gibert et al., 2007). A detailed explanation on the calibration strategy and accuracy/precision estimates is under preparation in an article from Xueref-Remy et al.(2013). The precision for the different datasets is given in Table 1. The temporal sampling is 1h for GIF and TRN stations, and 5 min for EIF, GON and MON.

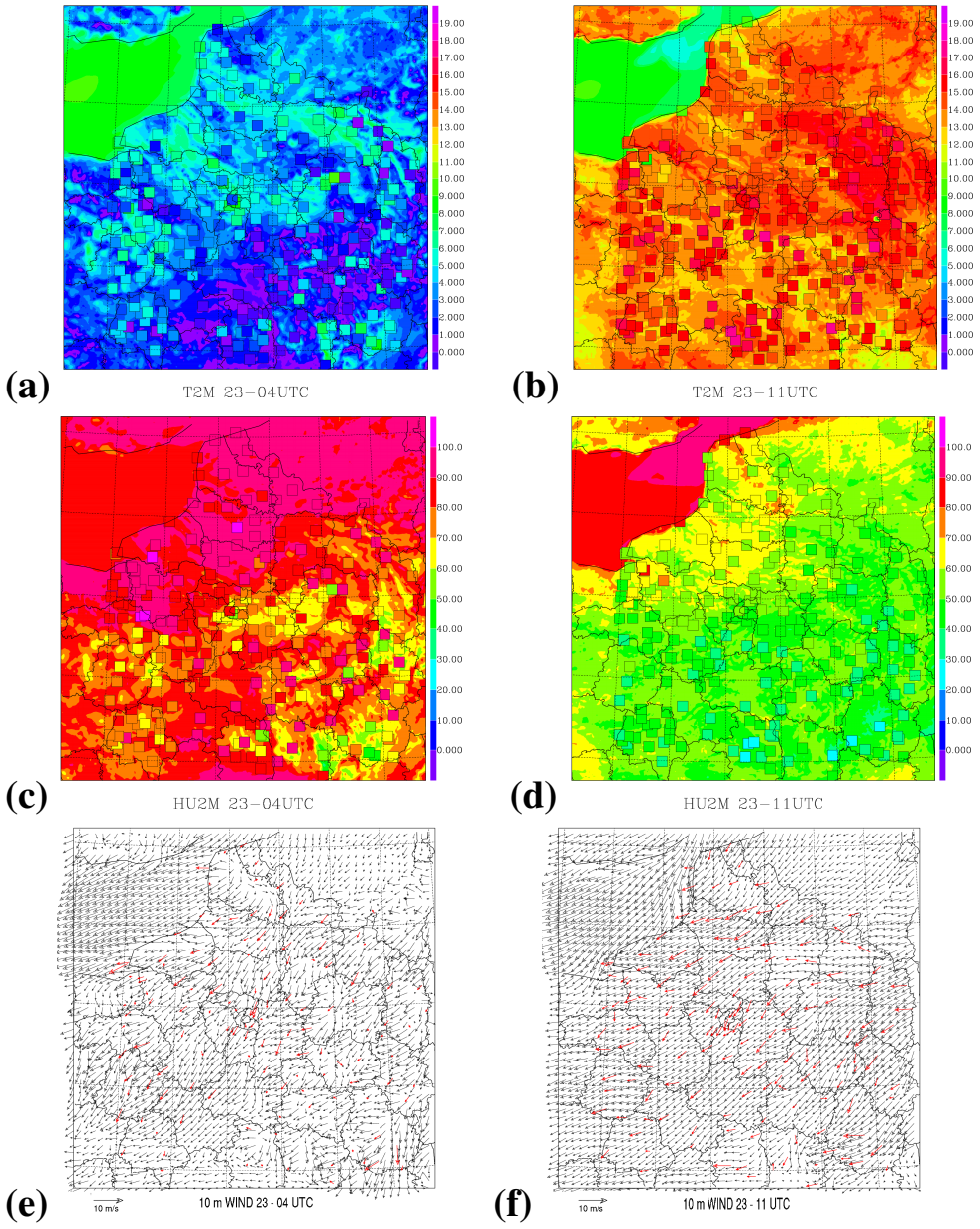

Fig. 2. MESO-NH predictions for 2 m relative temperature (in °C) (**a** and **b**), 2 m relative humidity (in %) (**c** and **d**) and 10 m wind (**e** and **f**) with observations shown by coloured squares/arrows for 23 March at 04:00 UTC (on the left) and 11:00 UTC (on the right).

The meteorology during the first 4 days of the study period was characterised by anticyclonic conditions over the north-west of Europe, maintaining dry and sunny weather over most of France. In the Paris area it led to weak north-easterly winds and temperatures progressively increasing and reaching a maximum of 21 °C on 24 March. On 25 March the winds became very weak due to the formation of a ridge between high-pressure regions stretching from the north-west of Ireland, through France, and past the southern tip of Italy. This ridge began to break up on 26 March as a low-pressure cell moved in from the Atlantic. In the Ile-de-France province, the wind rotated to the south-west and the sky became cloudy. This has resulted in two meteorological regimes during the study period, with the transition day between them on 25 March.

Table 1. Precision of the dataset (in ppm).

	EIF	GON	MON	GIF	TRN
Precision	0.382	0.065	0.101	0.500	0.500

Table 2. Dynamical and physical options used in the Meso-NH model.

Vertical coordinates	Gal-Chen and Sommerville
Basic equations	Non-hydrostatic, anelastic
Grid type	Arakawa C-grid
Transport schemes	WENO 3rd order for momentum
	PPM for meteorological and scalar variables
Time integration	2nd order Runge–Kutta split explicit
Time step	60 s for the physics
	15 s for the advection
Radiation	ECMWF scheme: rapid radiative transfer model longwave
	and Fouquart shortwave
Microphysics	Single moment class 5 Pinty and Jabouille (1998)
Turbulence	1-D Cuxart et al. (2000)
	with Bougeault and Lacarrere (1989) mixing length
Shallow convection	eddy-diffusivity mass-flux scheme
	Pergaud et al. (2009)

3 Modelling strategy with MESO-NH

The MESO-NH model (Lafore et al., 1998) is a non-hydrostatic mesoscale model developed by Meteo-France and Laboratoire d'Aerologie for research purposes (see http://mesonh.aero.obs-mip.fr/mesonh/). The model has been widely used to investigate the CO_2 cycle (Sarrat et al., 2007a,b, 2009; Noilhan et al., 2011). In this study the model has been run at 2 km horizontal resolution over a domain of 500 km $\times$ 500 km covering Northern France, the southeast of England and most of Belgium, as shown in Fig. 1a. The vertical resolution is minimum (18 m) near the surface and 2 km at the top of the domain above 20 km, leading to 46 levels with 21 levels in the first 2 km. An overview of the model set up, dynamical parameters and model physics used is given in Table 2. The atmospheric model assumes the CO_2 mixing ratio transported as a passive scalar.

The MESO-NH model runs in line with the land-surface–atmosphere interaction model SURFEX (Masson et al., 2012), including four components representing ocean, inland waters, urban areas and vegetation, corresponding to the surface types in the land cover ECOCLIMAP II (Masson et al., 2003), which has a resolution of 1 km and includes 273 ecosystems. The most important components included in the surface model for this study are the urban and vegetation schemes, the Town Energy Balance (TEB) (Masson, 2000) and Interactions between Soil, Biosphere, and Atmosphere (ISBA-A-gs) (Calvet et al., 1998; Noilhan and Planton, 1989) respectively. The TEB model was previously validated and has shown to reproduce well surface fluxes in urban areas both in offline mode (Hamdi and Masson, 2008) and online with MESO-NH (Masson, 2006; Lemonsu et al., 2006; Hidalgo et al., 2008). ISBA-A-gs includes CO_2 assimilation by the vegetation and ecosystem respiration to compute online the surface energy and CO_2 fluxes. The latent heat flux as well as the carbon flux are computed through a stomatal conductance. ISBA-A-gs uses a tile approach in which each grid cell is divided into a maximum of 12 patches of natural or vegetation types (bare soil, snow, rock, tree, coniferous, evergreen, C3 crops, C4 crops, irrigated crops, grassland and parks). Noilhan et al. (2011) have shown a significant improvement of the ABL representation by fully coupling CO_2 between surface and atmosphere using the tiling approach. The SURFEX scheme diagnoses the 2 m temperature and humidity, and 10 m wind with a specific algorithm (Masson and Seity, 2009) that implements a 1-D prognostic turbulence scheme on 6 vertical levels inserted between the surface and the lowest atmospheric model level (9 m here).

The anthropogenic CO_2 emissions are obtained from an inventory (10 km and 1 h resolutions) provided by the University of Stuttgart (Dolman et al., 2006). Oceanic CO_2 fluxes are parameterised following Takahashi et al. (1997), at the resolution of the model.

Each day of the campaign is simulated by a single 24 h model run, initialised and coupled every 3 h with the analysis from the 2.5 km resolution operational model of AROME (Seity et al., 2010) for the meteorological fields. The first day's CO_2 field was initialised with the CO_2 background mixing ratio measurement at the Eiffel Tower (minimum value of the day), with a homogeneous vertical profile, horizontally consistent across the entire model domain, while the other days used the predicted CO_2 field from the end of the previous day as a starting mixing-ratio field. The boundary conditions CO_2 profiles during each day's simulations were also taken from the Eiffel Tower measure, considering a homogeneous vertical profile. A sensitivity test on lateral boundaries for CO_2 has been led by using CO_2 fields from LMDZ model (with a horizontal resolution of 0.83° per 1.25° (latitude per longitude) over Europe), like in Ahmadov et al. (2009), but shows no significant impact on CO_2 prediction fields over the Paris region. In the future, this aspect could be improved by restoring the lateral boundaries toward

a large-scale analysis of CO_2, like MACC analysis (Engelen et al., 2009, see http://www.gmes-atmosphere.eu/about/project_structure/global/g_ghg/). Also, it is thought that for such anticyclonic situations, the effect of large-scale advection of CO_2 in the boundary layer is probably weak compared to the vertical turbulent diffusion. Additionally, the simulation domain is sufficiently large to minimise the lateral boundary condition effects in the domain of interest as it includes the main pollution sources influencing air quality over the Paris region, like Lille, industrial areas of Benelux and port activities of the Normandy coast.

Three simulations are performed using the same model configuration, i.e. same domains, initialisation fields and physical parameterisations: (1) the first simulation (henceforth REF, as the reference) is performed with the whole surface schemes; (2) the second simulation (RUR hereafter) is conducted without the TEB urban scheme in order to quantify the effect of the urban parameterisation: the urban land-use covers are replaced by rock, treated by ISBA, as the rock does not induce evapotranspiration that would modify the dynamics of the BL, and presents a significant roughness and non-erodible elements, like vegetation; (3) the third simulation corresponds to REF for the surface schemes, but without CO_2 anthropogenic emissions (hereafter NAN). In order to generalise the evaluation of the BLH, the REF simulation has been daily run for 1 yr (1 August 2010–31 July 2011) over the same domain, in exactly the same configuration.

4 Meteorological results

The performance of the Meso-NH simulations is first evaluated against boundary layer observations. The meteorological measurements considered are the following: (1) The 2 m air temperature (T2M) and relative humidity (HU2M) and 10 m wind fields observed at numerous meteorological stations: 235 stations reporting hourly data for T2M and HU2M and 114 stations reporting daily wind speed and wind direction are considered every day extending over the domain (Fig. 2). (2) T2M at urban (Paris-Montsouris), suburban (SIRTA) and rural (TRN) stations during the campaign. (3) The potential temperature vertical profiles and the BLH from the radiosounding (RS) at TRAP. (4) The BLH measured by the lidar systems at the 3 stations (TRN, SIRTA, JUSS).

4.1 Reference simulation evaluation: urban heat island (UHI)

Evaluating meteorological simulations against T2M, HU2M and 10 m wind fields is a very common practice in operational weather prediction centres. The scores against screen-level variables are generally difficult to improve and can be considered as very informative of the quality of the surface and boundary layer simulation. A synthesis of the mean biases and root-mean-square errors (rmse) is given in Fig. 3

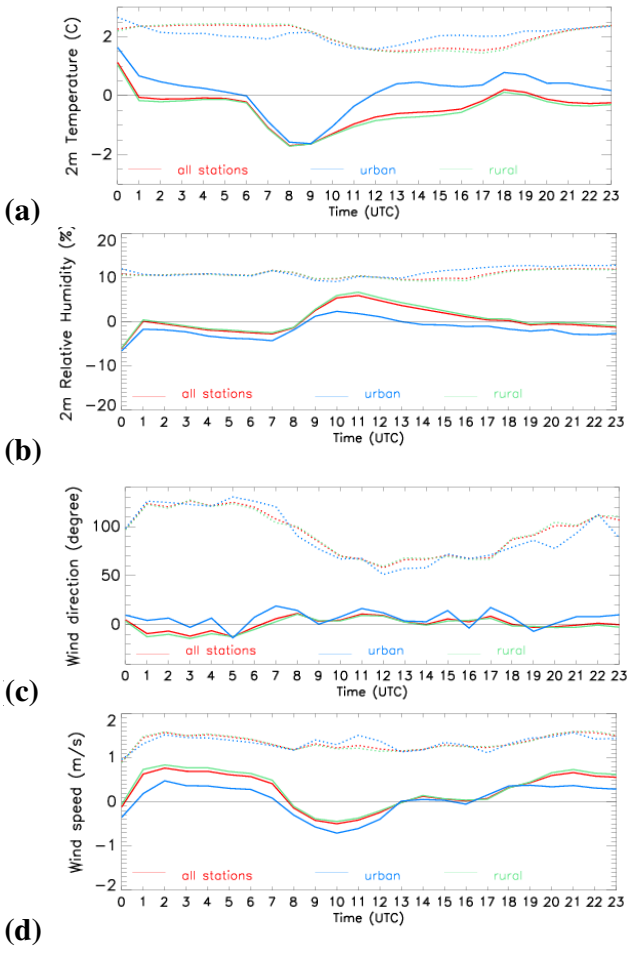

Fig. 3. Daily variation of the bias (solid line) and rmse (dashed line) for the REF simulations for the 2 m temperature **(a)**, 2 m relative humidity **(b)**, 10 m wind direction**(c)** and speed **(d)**, considering all the stations (in red), or decomposed between urban (in blue) and rural stations (in green). Urban stations represent 35 stations over 235 stations for T2M, 33 stations over 182 stations for HU2M and 27 stations over 113 stations for the 10 m wind fields.

for the REF simulation. In order to evaluate separately TEB and ISBA schemes, the scores are separated between urban and suburban stations on one side (corresponding to a town fraction greater than 0.1, leading to 35 stations over 235 for T2M) and rural stations (town fraction less than 0.1) on the other side. Statistical scores show a good behaviour of the REF simulation, with a bias less than 1.8 °C for T2M, 6 % for HU2M, 0.8 m s^{-1} and 20° for the wind speed and direction, respectively. The deviation from the measurements (rmse) is a bit higher. There is an indication of diurnal trend in the statistics of bias: for all stations (red curve), the predicted atmospheric regime is slightly too cold and too wet during the day, but in very good agreement at night, as illustrated on Fig. 2 for 23 March at 04:00 and 11:00 UTC. For urban stations, a small positive bias appears on temperature and humidity during the whole day except the morning,

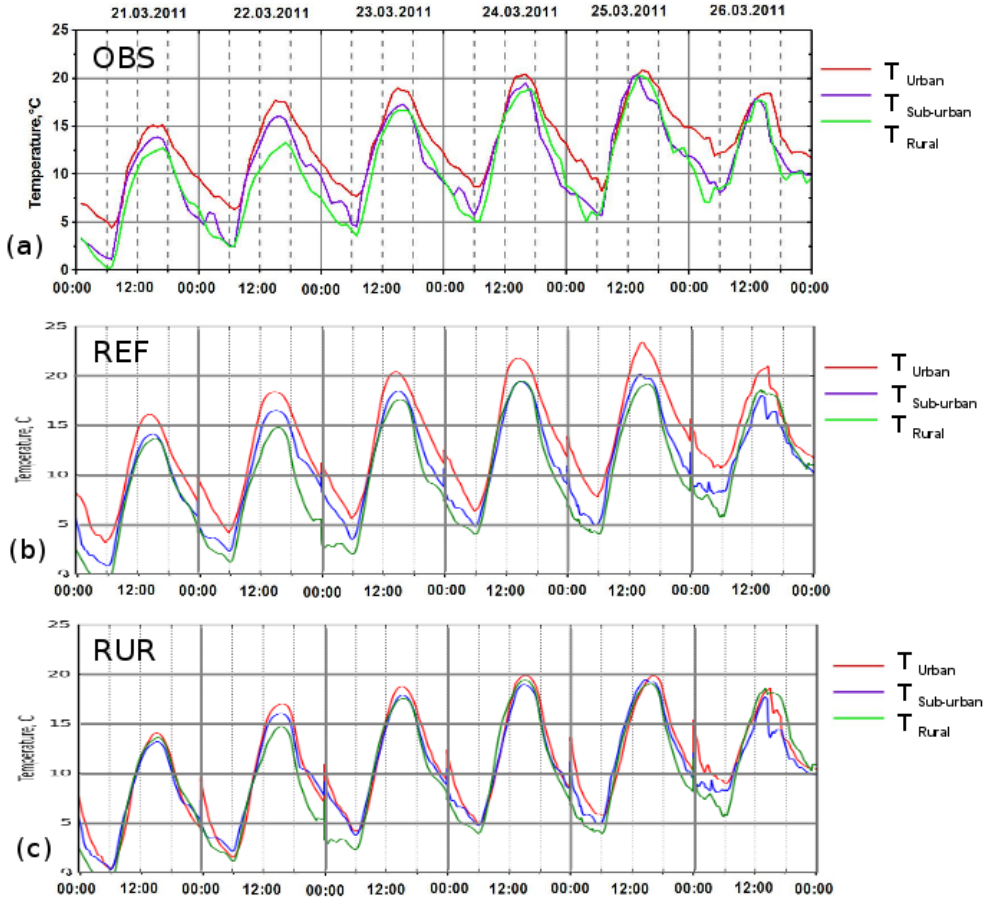

Fig. 4. Diurnal variation of hourly near-surface air temperature (in °C) at urban, suburban and rural stations measured (from Pal et al., 2012) **(a)**, predicted with REF simulations **(b)** and RUR simulations **(c)**.

meaning that the TEB scheme tends to overpredict the UHI by up to 0.5 °C during the night. A possible explanation is that the surrounding of urban stations is often characterised by a high portion of urban vegetation that is underestimated at 2 km horizontal resolution and by the 1 km ECOCLIMAP data. Also, the parks and vegetated spaces embedded in an urban/suburban surrounding are not considered by the TEB scheme; this will be a further improvement of the urban parameterisation (Lemonsu et al., 2012). On the contrary, the excessive surface cooling and moistening during the day is probably relative to the ISBA scheme. Deviations from the measurements (rmse) are equivalent for urban and rural stations. The wind speed is slightly overestimated during the night, especially on the rural stations, and underestimated at the end of the morning, particularly for urban stations. The error in the wind direction is small and fluctuating, with a high deviation, due to the fact that the wind speed is very weak during the period, making the prediction difficult. Scores are very similar for all the days of the period (not shown).

Figure 4 shows the time series of the near-surface air temperature measured and predicted at urban (Paris-Montsouris), suburban (SIRTA) and rural (TRN) stations during the campaign. The upper panel exemplifies the classical diurnal cycle of observed temperature, with here an increasing trend over all sites until 25 March and a change during 26 March. The daily maximum temperature observed at Paris increased from 15 °C on 21 March to 21 °C on 25 and decreased to 17 °C on 26, while the minimum temperature increased from 5 °C on 21 March to 14 °C on 25 March, and remained constant on 26 March. The higher increase of minimal temperatures than maximal temperatures is a signature of the thermal accumulation effect in the urban area (Pal et al., 2012). The observed differences of temperature between the urban site on one side, and the suburban and rural sites on the other side, representative of the UHI, are presented on Fig. 5. They were most of the time positive and can reach 5 °C and 7 °C, respectively. They were stronger at night than during day and, mostly, the contrast between the three sites was negligible during sunrise. The highest nocturnal UHI between urban and rural sites occurred on 26 March with a difference of 7 °C, whereas the difference was slightly negative 12 h before, during 25 March afternoon, due to the absence of wind inducing a generalised strong heating over

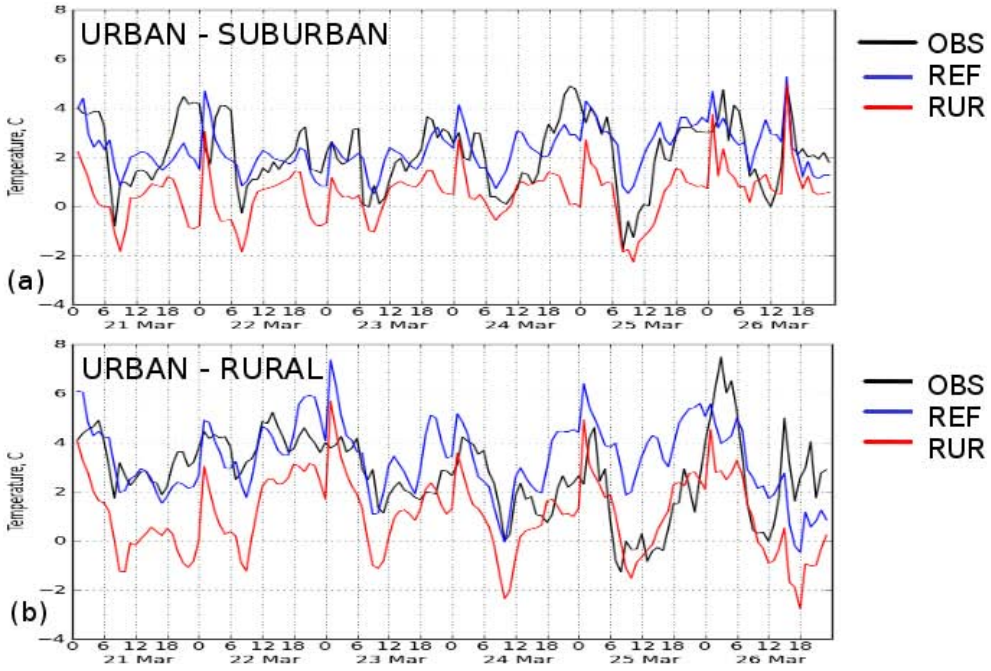

Fig. 5. Diurnal variation of hourly differences of temperature at 2 m (in °C) between urban and suburban stations **(a)** and between urban and rural stations **(b)** from observations (in black), REF (in blue) and RUR (in red) simulations.

Table 3. Evaluation of the mean bias, rmse (in $°C$) and correlation coefficient (R^2) between observations and REF and RUR simulations on T2M at Montsouris (URBAN), SIRTA (SUBURBAN) and Trainou (RURAL) sites

URBAN			
	BIAS	RMSE	R^2
REF	+ 0.8	1.6	0.9
RUR	− 3.0	2.9	0.75
SUBURBAN			
	BIAS	RMSE	R^2
REF	0.0	1.0	0.96
RUR	− 0.5	1.4	0.92
RURAL			
	BIAS	RMSE	R^2
REF	− 0.2	1.5	0.93
RUR	− 0.2	1.5	0.93

all the domain. Also, the dry conditions that prevailed the previous days reduced the soil moisture at the rural site, and evapotranspiration by the vegetation became therefore small during daytime.

The middle panel of Fig. 4 represents the predicted temperature on the same sites for the REF simulation. The discontinuity sometimes present at 00:00 UTC for the different days corresponds to the analysis from AROME model that initialises the new Meso-NH daily simulation. It is noteworthy that, between the 3 sites, only the measurements at Paris-Montouris are included in the data assimilation in AROME, inducing the same T2M between observation (Fig. 4a) and initial conditions of the run (Fig. 4b) at 00:00 UTC – contrary to the measurements at SIRTA and TRN sites, which do not include the operational meteorological surface observation network, so are not taken into account in the data assimilation system to produce the operational analysis. The REF simulation reproduces well the increasing trend in temperature (Table 3, with correlation R^2 between 0.9 and 0.96 for the 3 stations), with nevertheless a systematic overestimation of the maximum temperature at the urban site of 2 °C (inducing a mean bias of +0.8 °C). Indeed, Montsouris station is a good example of an urban station embedded in a park, whose effects on surface fluxes are not considered, as mentioned before.

The UHI intensity is fairly well represented by the REF simulation (Fig. 5), with a good range of values, and maxima during the nights and minima during the days. The main discrepancy concerns the absence of urban–rural contrast observed during the day of 25 March, which is not captured by the model, and the maximum observed UHI during the following night that is underestimated (5 °C instead of 7 °C).

These results illustrate the fact that the REF simulations closely match the observations and can capture the urban–rural contrasts in temperature fairly well.

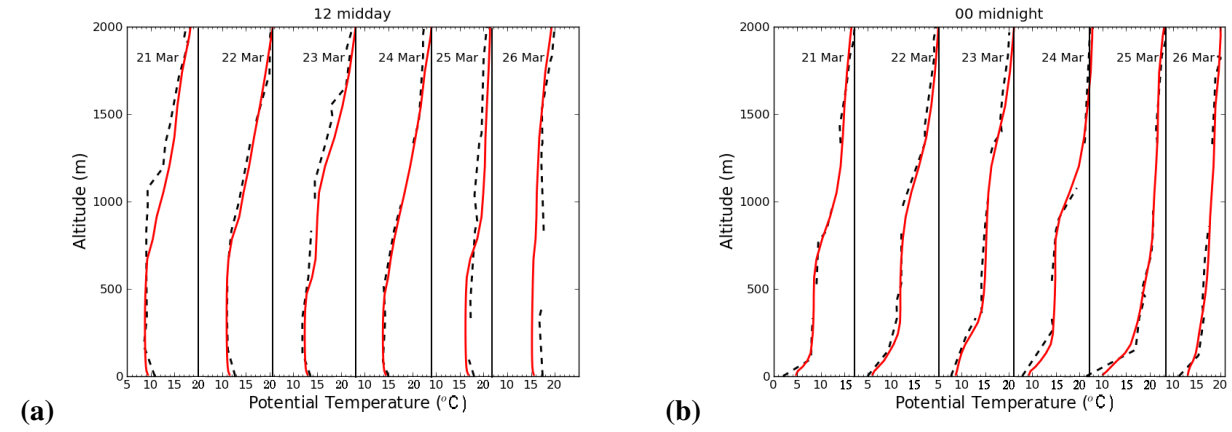

Fig. 6. Vertical profiles of potential temperature (in °C) above the Trappes location for 12:00 UTC **(a)** and 00:00 UTC **(b)** for the measurements (black dashed lines) and REF simulations (solid red lines).

4.2 Boundary layer height (BLH)

Figure 6 shows vertical profiles of potential temperature above TRAP at 00:00 and 12:00 UTC for the REF simulation, compared to the daily soundings. The sonde drifting has been neglected for the simulation comparison as the wind in the ABL is weak during the period. In agreement with the previous scores, the surface temperature at this suburban site tends to be slightly underestimated during the day and overestimated during the night. At midday the convective mixing is fairly well reproduced, except on 21 March, where the BLH is slightly underpredicted. At midnight the nocturnal positive potential temperature gradient is generally well represented with, however, a small underestimation on 25 and 26 March inherent to the small positive bias on surface temperature. Steeneveld et al. (2008) have underlined the frequent underestimation of the stratification of nighttime surface inversions in mesoscale models, pointing out the difficulty in parameterising stable boundary conditions. However, the model tends to capture well the potential temperature profiles. To evaluate more accurately the BLH predictions, BLH are extracted from lidar and ceilometer measurements, following the method discussed in Pal et al. (2010), and compared to the model diagnostics. The diagnosis of the BLH in the model is based on the bulk Richardson number approach (Seibert et al., 2000), considering a critical value of 0.25 (Sorensen et al., 1996). For 25 and 26 March the lidar was not working at SIRTA site due to technical problems and therefore only the ceilometer was used, reducing the quality of BLH estimation. Also, the lidar system was not operational over the rural site during nighttime since full overlap of the lidar system is reached at a height of around 150 m AGL.

Figure 7 shows time series of the BLH for the urban (JUSS), suburban (SIRTA) and rural (TRN) sites, with comparison between observations and simulations. During daytime, measurements show significant contrasts between the 3 sites with the deepest mixing for JUSS, followed by SIRTA and then TRN. However, for the first 4 days, these differences were limited (maximum of 200 m between JUSS and TRN), and the maximum BLH remained quite constant for all the days even if the near-ground temperature increased (Fig. 4a). The highest contrast on BLH between urban and rural sites during daytime occurred on 25 March with a difference of 600 m at 14:00 UTC, while near-ground surface temperatures differed only from 1 °C between rural and urban sites. This was probably due to high values of daytime evapotranspiration at TRN. 26 March was characterised by a weaker BLH than the previous day and some fluctuations at SIRTA and TRN due to the change in the prevailing meteorological regime. During nighttime, where the BLH is determinant for the pollutant mixing ratios, measurements showed maximum BLH differences between JUSS and SIRTA sites of the order of 100 m.

The REF simulation captures reasonably well the BLH for all the sites with correlation coefficients between 0.89 at JUSS and 0.71 at TRN (Table 4). During daytime, biases are negative between 8 m (at TRN) and 70 m (at JUSS). This can be explained for the rural site by the small negative bias on T2M (Fig. 4). In the morning the onset time of the ABL mixing and the growth rate of the BLH are particularly well reproduced (Fig. 7). Maxima of BLH are also well captured, except a large underprediction on the 1st day for the 3 sites (up to 300 m at JUSS) and a small one on the 4th day at JUSS and TRN. The increase of daytime BLH on 25 March, compared to the other days, is predicted at the 3 sites, but slightly underestimated at SIRTA and overestimated at TRN. During nighttime the REF simulation represents fairly well the shallow mixing depth over urban and suburban sites, but tends to underestimate it slightly (negative biases of 45 m and 5 m respectively, Table 4).

The evaluation of BLH has been generalised over the 1 yr period by comparisons against BLH from daily soundings at

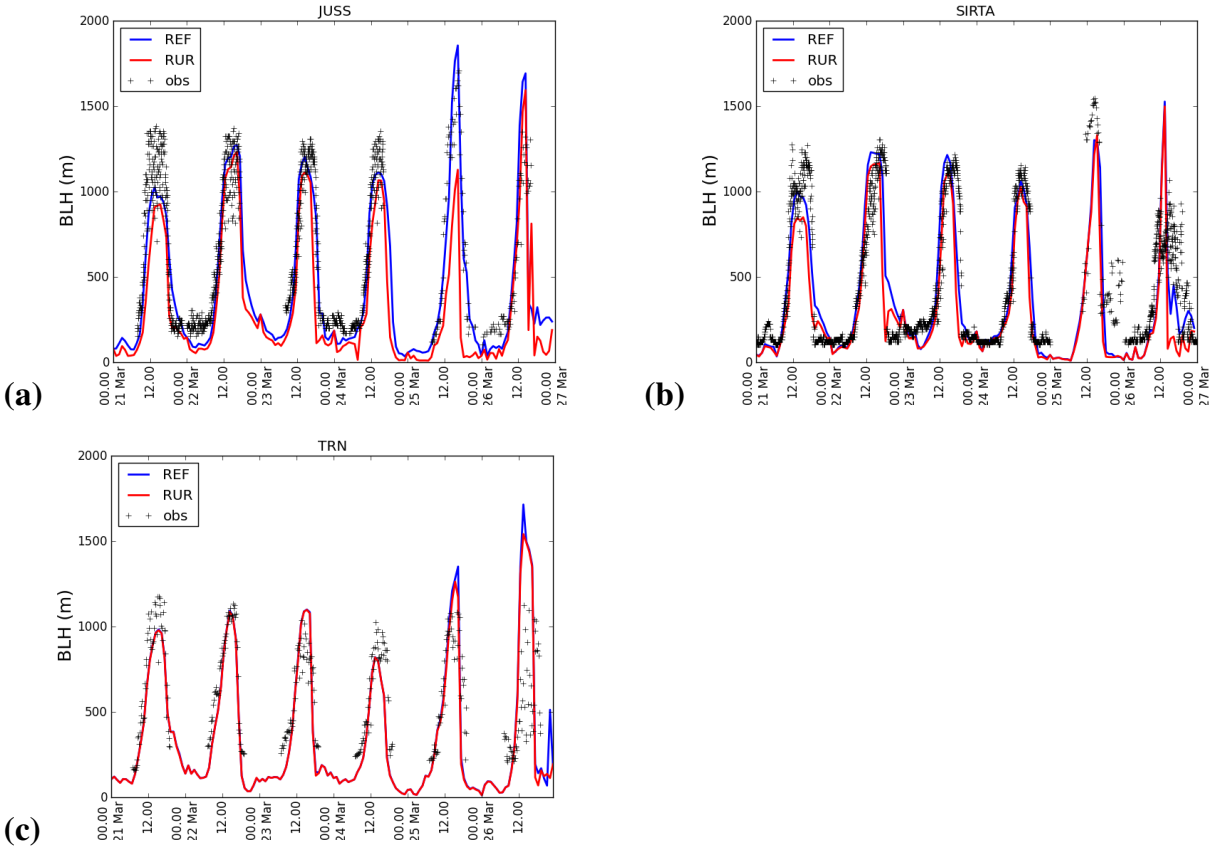

Fig. 7. Time series of BLH (in metres a.g.l. (AGL)) for 21–26 March at JUSS (**(a)**, urban site), SIRTA (**(b)**, suburban site) and TRN (**(c)**, rural site).

Table 4. Mean observed, bias, rmse and correlation coefficient (R^2) of the BLH for the REF and RUR simulations. Nighttime is considered from 19:00 UTC to 08:00 UTC.

JUSSIEU					
	Mean Day		Mean Night		
OBS	867		222		
Simul.	Bias Day	Rmse Day	Bias Night	Rmse Night	R^2
REF	−70	222	−45	131	0.89
RUR	−226	320	−117	132	0.78
SIRTA					
	Mean Day		Mean Night		
OBS	731		155		
Simul.	Bias Day	Rmse Day	Bias Night	Rmse Night	R^2
REF	−34	256	−5	127	0.76
RUR	−160	313	−44	106	0.68
TRN					
	Mean Day				
OBS	661				
Simul.	Bias Day	Rmse Day			R^2
REF	−8	303			0.71
RUR	−23	293			0.72

TRAP, also estimated with the same critical bulk Richardson number. Correlation are presented in Fig. 8 with the regression line included, and biases and rmse are reported in Table 5. Statistics reveal very good agreement at this suburban site, with biases of +19 m and −6 m for 12 h (12:00 UTC soundings) and 24 h (00:00 UTC soundings) forecasts, respectively. But we can underline that statistics on SIRTA and TRAP agree on the fact that the model tends to underestimate slightly the nocturnal BLH at suburban sites. The mean diurnal cycle exhibits good agreement between observation and REF at noon and midnight (Fig. 8c).

4.3 Importance of the urban scheme

The evaluation of the RUR simulations is compared to the REF ones for T2M, HU2M and 10 m wind at the urban stations (Fig. 9). The absence of an urban scheme logically translates the bias curve to weaker temperatures (higher humidities) similarly for each hour, increasing the negative bias of T2M (positive bias of HU2M) during the day and reducing the positive bias of T2M (negative bias of HU2M) during the night. It also increases slightly the negative biases of the wind speed during the day, meaning that the absence of urban–rural contrasts on temperature reduces the wind. The

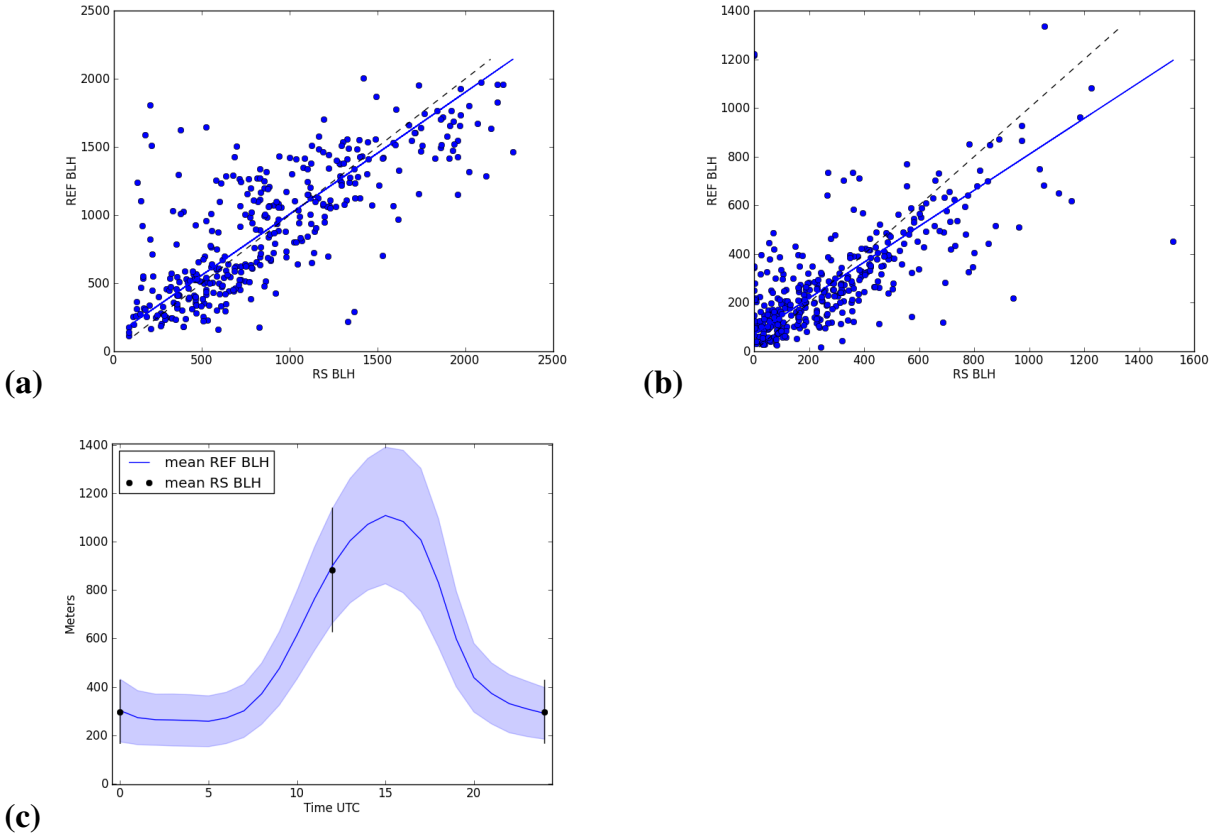

Fig. 8. (a) and **(b)**: Correlation between observed (noted RS) and simulated BLH at Trappes for the REF simulation for 1 yr (August 2010–July 2011) for 12 h forecast (12:00 UTC sounding) and 24 h forecast (00:00 UTC sounding). The regression is indicated by the continuous line. **(c)**: Diurnal cycle over the year of the BLH at Trappes predicted by REF (blue line for the mean and blue area for the standard deviation) with the observed values marked by dots for the mean and by bars for the standard deviation.

Table 5. Statistical scores of the BLH at Trappes from observation (mean and standard deviation, noted STD DEV) and from the REF simulation over 1 yr (August 2010–July 2011).

TRAPPES (BLH in m)				
	MEAN 12:00 UTC	STD DEV 12:00 UTC	MEAN 00:00 UTC	STD DEV 00:00 UTC
OBS	883	515	296	265
REF	902	473	290	213
	BIAS 12H Forecast	RMSE 12H Forecast	BIAS 24H Forecast	RMSE 24H Forecast
REF	+ 19	337	− 6	191

discrepancies in the wind direction are also increased without the urban scheme. The absence of an urban scheme has therefore a negative impact as it removes the urban–rural contrasts, and the associated circulations (Hidalgo et al., 2008). On Fig. 4c the RUR simulation underestimates systematically the urban temperature (Table 3 with a negative bias of −3°C), the corrections by the analysis at 00:00 UTC are important and it removes the UHI (Fig. 5 in red line). However some contrasts between the three sites remain that are only linked to the orography effect of the Paris Basin and to the cooling associated to the evapotranspiration for the rural site compared to the rock replacing the urban area in the RUR simulation.

The comparison between REF and RUR simulations on the BLH (Fig. 7) shows a systematic reduction of the BLH at the urban site during the day and during the night, degrading significantly the negative biases and the correlation (Table 4). At the suburban site, the difference between both is reduced compared to the urban site but not negligible, as evidenced by the statistics, especially on the maximum of the afternoon

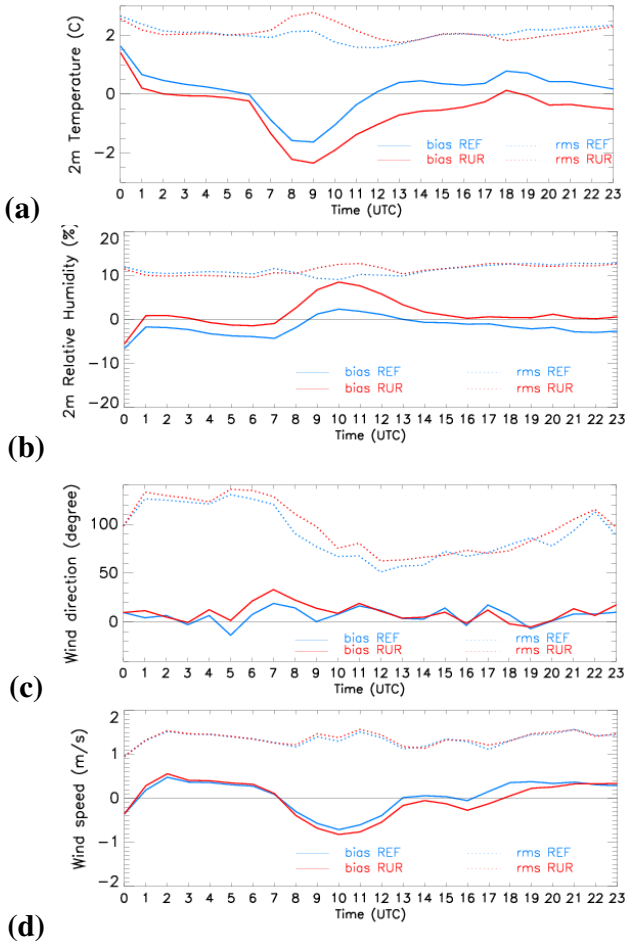

Fig. 9. Daily variation of the bias (solid line) and rmse (dashed line) for the REF (in blue) and RUR simulations (in red) for the 2 m temperature **(a)**, 2 m relative humidity **(b)**, 10 m wind direction **(c)** and 10 m wind speed **(d)** only for the urban stations.

underestimated. At the rural sites curves are superimposed. This comparison demonstrates the effectiveness of the TEB scheme in representing urban–rural contrasts on the BLH.

5 CO_2 distribution in regional scale

CO_2 mixing ratio predictions are investigated herein using time series of predictions from REF, RUR and also NAN simulations against observations for the Eiffel Tower (hereafter EIF), Gonesse (GON), Montge-en-Goelle (MON), Gif-sur-Yvette (GIF) and Trainou (TRN). The NAN simulation allows distinguishing the sites quasi-fully influenced by anthropogenic emissions (EIF) and those strongly influenced by anthropogenic emissions (GON and GIF), as well as the site both exposed to anthropogenic and biogenic emissions (MON) and finally the rural site quasi-fully driven by photosynthesis and plant transpiration (TRN). It is worth noting that peak values of anthropogenic emissions over Paris and its airports occur during rush hours – between 05:00 and 08:00 UTC (local wintertime), and 18:00 and 22:00 UTC (not shown). But nocturnal emissions remain important at CDG Airport as it is today the airport with the leading European night traffic, with an average of 170 movements per night (almost 15 % of the total of the airport traffic over 24 h).

5.1 Evaluation at the urban site: Eiffel Tower

The mean diurnal cycle is presented in Fig. 10a. for EIF. The observed CO_2 maxima occur much later than for the other sites, generally between 09:00 UTC and 11:00 UTC. While the other sites record the highest concentrations when the BLH is fully contracted, the Eiffel Tower concentrations show maxima during the late morning as the ABL expands. As JUSS is close to EIF, observed and predicted BLH evolutions at JUSS are used to help in analysing CO_2 observations and predictions at EIF (Fig. 11). The observed CO_2 spikes trigger exactly at the time (vertical dashed line) at which the growing BLH reaches the measurement height of the Eiffel Tower (310 m, as shown in Fig. 11a). These spikes have a very short duration as the ABL grows quickly, favouring the rapid mixing of pollutant in a deeper layer, and consequently the rapid CO_2 mixing ratio decreases. In terms of timing and temporal evolution, the modelled mixing ratios can be seen to agree well with observations: predicted and observed maxima occur at the same time, meaning that the predicted BLH reaches 310 m at the right time. The predicted CO_2 peaks are also very brief, in agreement with measurements. The correct timing is confirmed on the mean diurnal cycle (Fig. 10a). However, a few discrepancies appear in the temporal evolution. Firstly, the longest period of high observed mixing ratios has occurred during the night of 22–23 March. It is underestimated by the model, probably due to an underprediction of the BLH (measurements at JUSS were not available), even if the REF simulation tends to produce higher BLH than for the other nights, reaching punctually the EIF measurement height. Secondly, another discrepancy occurs on 25 March at 02:00 UTC as the model predicts a peak of 450 ppm that does not occur in reality, associated to a reservoir of pollutant in the simulated residual layer. All of this can explain that statistically, the comparison model vs observation gives a negative bias of 6 ppm (rmse of 17 ppm) and a middling 0.35 correlation coefficient (Fig. 12a). In terms of intensity, another discrepancy concerns the strongest peak event measured at EIF during the campaign (25 March at 11:00 UTC), slightly underestimated by the model. This peak is a consequence of the negligible wind during all the night and the early morning (Fig. 13): anthropogenic CO_2 accumulates over Paris Intra-Muros in the Seine Valley in the shallow early morning ABL (Fig. 13c at 08:00 UTC) and this reservoir reaches 300 m height with the ABL growing at 11:00 UTC (Fig. 13d). The model underpredicts the maximum over the Eiffel Tower, even if predicted winds are in agreement with observations at the ground and

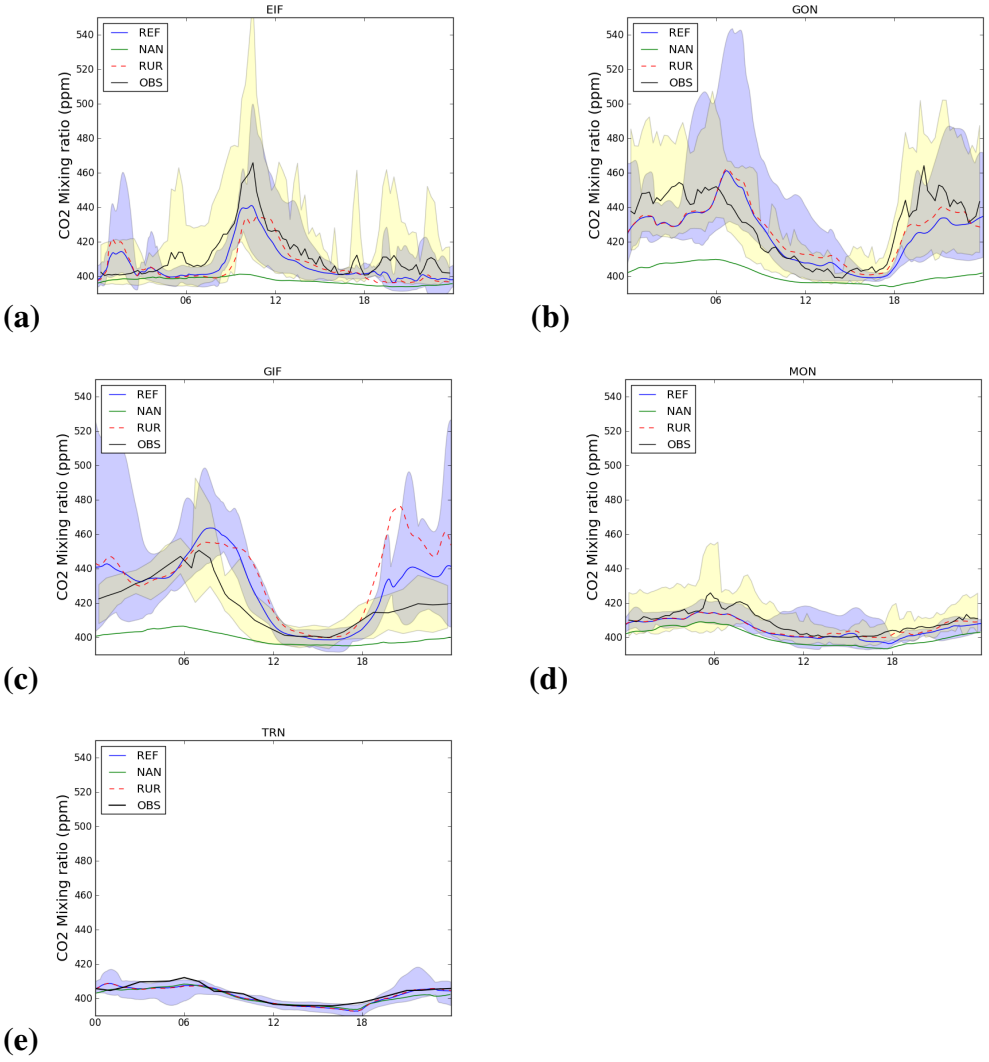

Fig. 10. Mean temporal evolution (over 6 days) of the CO_2 mixing ratios (in ppm) measured (black line) and predicted with REF (blue line), RUR (red line) and NAN (green line) simulations at EIF **(a)**, GON **(b)**, GIF **(c)**, MON **(d)** and TRN **(e)**. The yellow area is between the minimum and maximum of the measurements, and the blue area between the minimum and maximum of the REF simulation.

at 300 m height (Eiffel station), but reproduces CO_2 mixing ratio magnitudes at 300 m comparable to the measurements magnitude over the eastern part of Paris city (Fig. 13f with measurement in coloured square). The predicted plume mixing ratios are directly linked to the CO_2 emissions that are higher on the eastern part of Paris. It is therefore likely that the underestimation at EIF is partly due to the too coarse anthropogenic emissions as the correct mixing ratios have been produced on another part of Paris, and partly to horizontal transport errors, frequent with weak winds. Moreover, the simulated ground level mixing ratios closely match the lower observed mixing ratio values at the suburban sites (Fig. 13e). So the general anthropogenic pollutant accumulation over Paris city on 25 March is correctly reproduced, and its representation at local scale could probably be improved with finer emission inventories.

The RUR tends to delay by 30 min the peak of CO_2 (Fig. 10a) as the growing phase of the BLH is delayed by the same time (Fig. 7a). The misrepresentation of nocturnal UBL with RUR does not impact CO_2 concentration at EIF as the measurement is located above. Overall, the statistics are worse, with a correlation coefficient of 0.05 (Fig. 12b).

5.2 Evaluation at the suburban and rural sites

CO_2 mixing ratio observations and predictions at the suburban and rural sites are presented in Fig. 10 in terms of diurnal cycle and compared for statistics in Fig. 12. Contrary to the EIF altitude station, the surface suburban sites (GON and GIF) always measure maxima in the second part of the night and in the early morning, when the BLH is strongly

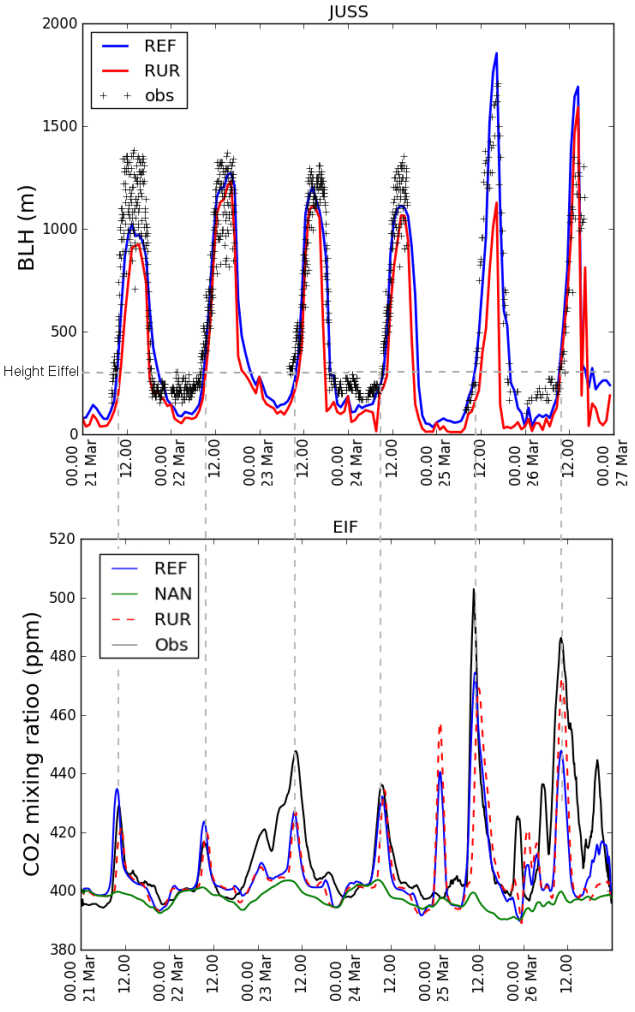

Fig. 11. (a) Time series of BLH predictions and observations at JUSS (in m a.g.l., AGL) for REF (blue) and RUR (red) simulations. **(b)** Time series of CO_2 observations and predictions (in ppm) at EIF for REF (blue), RUR (red) and NAN (green) simulations, hourly averaged. The vertical dashed lines correspond to the time in the morning at which observed BLHs reach 310 m (Eiffel measurement height).

contracted. They exhibit a strong temporal variability of CO_2 mixing ratio (yellow area in Fig. 10).

At GIF site (Fig. 10c), the REF simulation reproduces correctly the timing of the diurnal cycle of CO_2 mixing ratio. But if the minimal CO_2 mixing ratios are well captured by the model, the nocturnal maxima tend to be overestimated, inducing a positive bias of 9 ppm and a correlation coefficient of 0.6 (Fig. 12c). This can be directly linked to the vertical transport error as SIRTA exhibited a negative bias of 5 m on the BLH. The RUR simulation degrades significantly the statistics (R^2 is equal to 0.22 and bias to +17 ppm) as shown on the diurnal cycle: the reduced mixing in the BL without TEB extends the period of strong CO_2 in the morning and at the end of the afternoon, and the lower nocturnal BLH increases the concentrations.

At GON, observation and REF simulation are in fairly good agreement with a correlation of 0.95 and a small negative bias of 4 ppm (Fig. 12e), and the diurnal cycle is well reproduced (Fig. 10b). The discrepancies mainly concern the maximum of the CO_2 peak in the early morning and the temporal evolution insures that only 25 March morning is imputed (not shown). On 25 March at 08:00 UTC, the near ground temperature on the north-east of Paris (Fig. 13a) is underestimated, inducing an error on the vertical transport leading to an overestimation of the mixing ratio (Fig. 13b). On the contrary, REF tends to underestimate the nocturnal concentrations (Fig. 10b). During a major part of the March period, GON experienced the plume of CDG airport during the night, in an east flux, as the airport kept up its night traffic activity. Therefore, the horizontal transport on one side and the uncertainties on the emission on the other side are two main potential sources of error of CO_2 at this station.

The MON station is classified as a rural site, but is nevertheless influenced by anthropogenic emissions from Paris and CDG airport as the difference between REF and NAN simulations is not negligible (Fig. 10d). The period exhibits two regimes, with a quite regular diurnal cycle the first 4 days and north-east winds that protect the site from Paris and CDG plumes, as on Figs. 14a and 15a, and a stronger variability the last 2 days due to the weak winds with variable directions, including mainly westerly winds (Figs. 14b and 15b). The model reproduces fairly well the CO_2 concentration, with a correlation of 0.7 and a negative bias of 4 ppm (Fig. 12g), but the second period was more exposed to horizontal transport errors and emission uncertainties. This is underlined by the statistics on the RUR simulation, which unusually does not degrade the scores (Fig. 12h), meaning that vertical transport errors are less involved.

While almost no observations are available for the rural site of TRN during this period, the measurements at the beginning of the period allow verification of the predicted mixing ratio. The CO_2 diurnal cycle is almost identical each day of the period, with a nocturnal maximum due to the ecosystem respiration (Fig. 10e), and a CO_2 mixing ratio decrease in the ABL when the BLH increases, due not only to CO_2 vertical mixing but also to photosynthesis activity which depletes the boundary layer CO_2 mixing ratio. The three simulations REF, RUR and NAN are almost superimposed, meaning that the vegetation fully drives the diurnal cycle of carbon.

5.3 CO_2 horizontal heterogeneity in the afternoon and the night for inversion purposes

Figure 10 shows that the model reproduces well the midday lower CO_2 mixing ratios at the different sites. Even if strong convective mixing in the ABL during daytime induces lower mixing ratio values, the horizontal flow can lead to

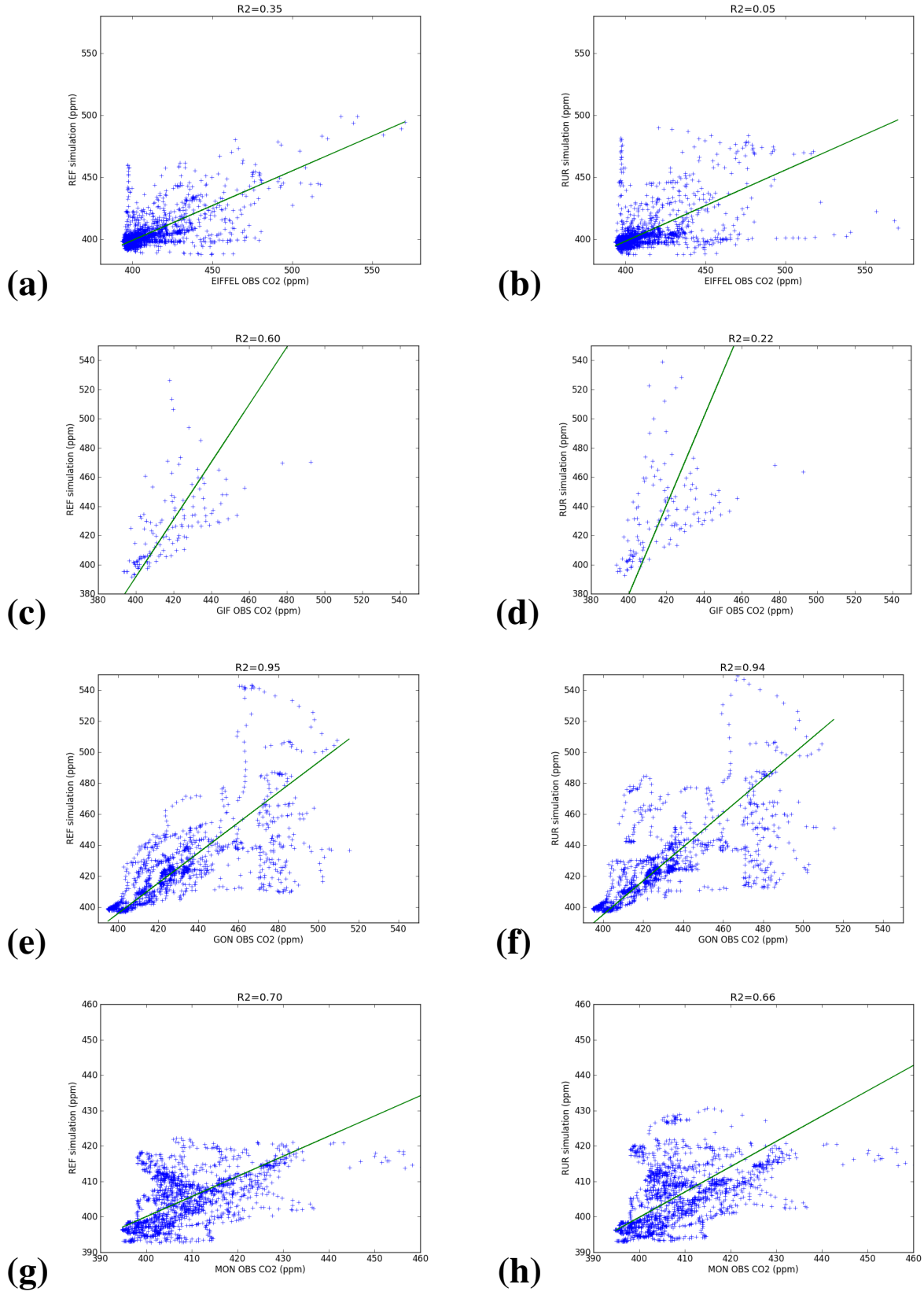

Fig. 12. Scatter plots of the observed (on the horizontal) vs predicted CO_2 mixing ratios for EIF, GIF, GON and MON for REF simulation (on the left) and RUR simulation (on the right), with a linear regression.

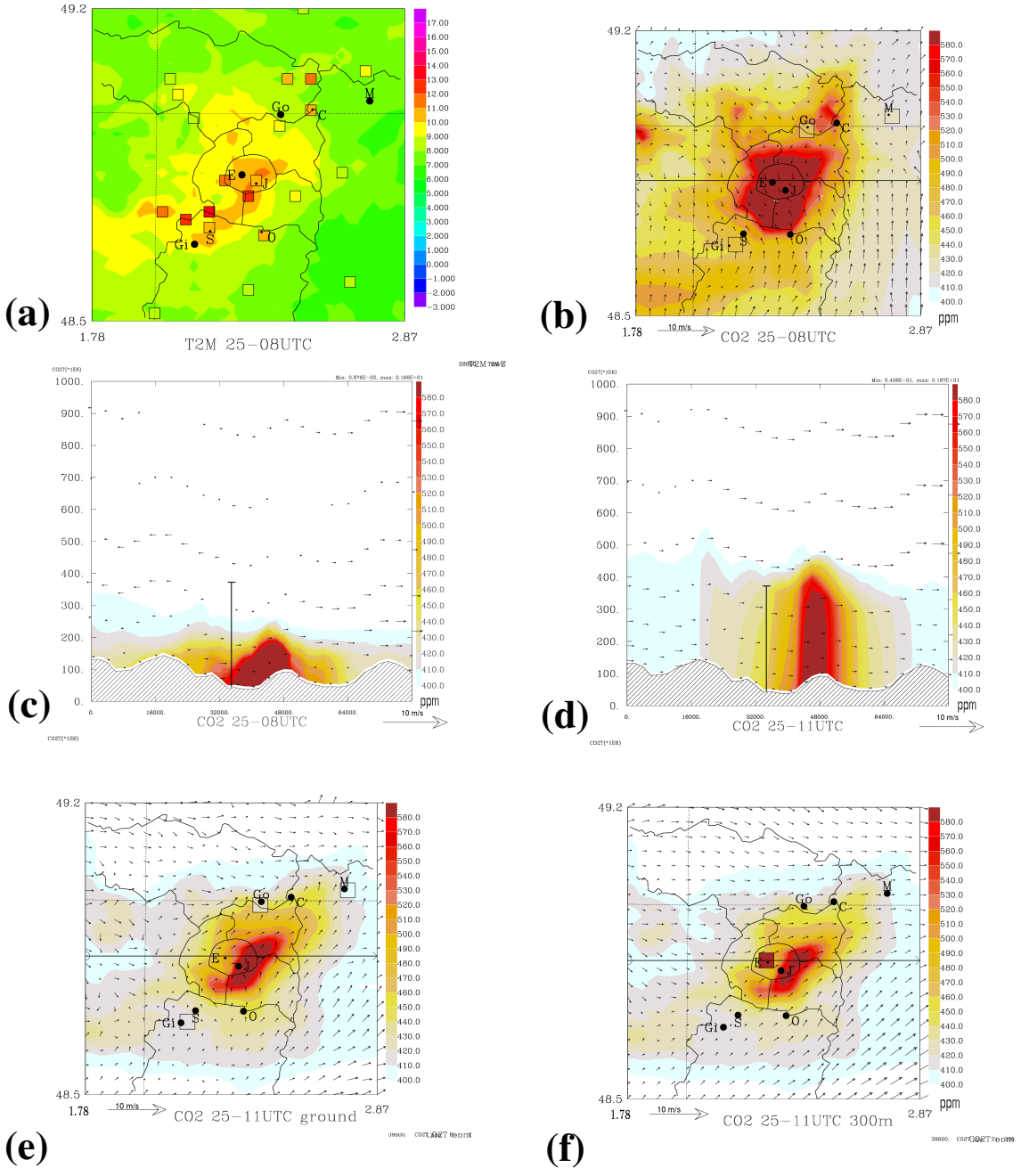

Fig. 13. MESO-NH predictions: for 25 March at 08:00 UTC **(a)** 2 m temperature (in °C), **(b)** Horizontal cross section of CO_2 mixing ratio (in ppm) near the ground. **(c)** Vertical cross section of CO_2 mixing ratio (in ppm) according to the axis given in **(b)** for 25 March at 08:00 UTC, and for 25 March at 11:00 UTC **(d)**, with wind vectors superimposed. The Eiffel tower is symbolised by a stick, with a length corresponding to its measurement height. Horizontal ticks indicate metres. For 25 March at 11:00 UTC: horizontal cross section of CO_2 mixing ratio (in ppm) near the ground **(e)** and at 300 m height **(f)** with wind arrows superimposed. Coloured squares mean observed CO_2 mixing ratio.

significant horizontal differences in CO_2 concentration. The first 4 days, the north-east flux induces a CO_2 concentration increase from GON to GIF, as illustrated on Fig. 14a, whereas it is reversed the next 2 days in the south-west flux (as illustrated on Fig. 14b). For instance, on 25 March at 15:00 UTC, observed horizontal CO_2 increments reach up to 15 ppm between GIF and GON, and this is quite well reproduced by the model (Fig. 14b). The predicted mixing ratio over MON is overpredicted by 10 ppm, but the station is located on the border of the predicted plume. Both the insufficient spatial accuracy of the anthropogenic emissions and errors on the horizontal transport (observed winds are

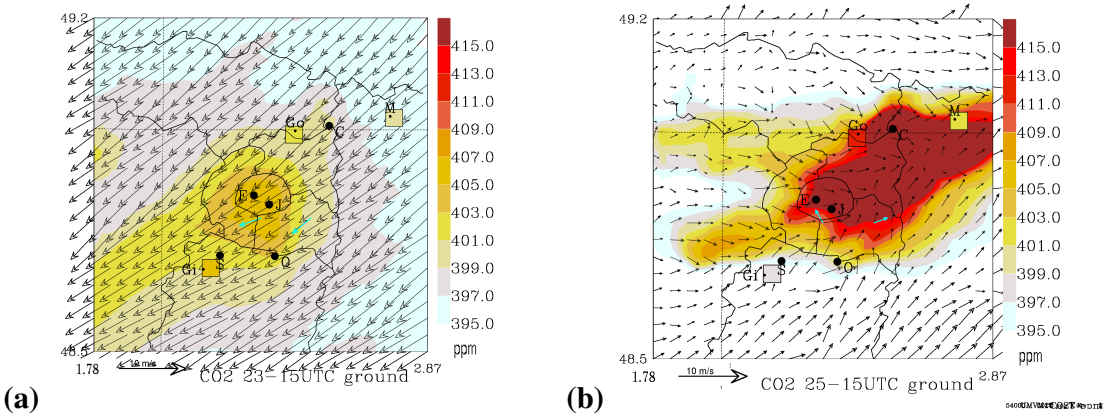

Fig. 14. Horizontal cross sections of CO_2 mixing ratio (in ppm) and predicted wind arrows (in m s^{-1}) near the ground for **(a)** March 23 at 15:00 UTC, **(b)** 25 March at 15:00 UTC

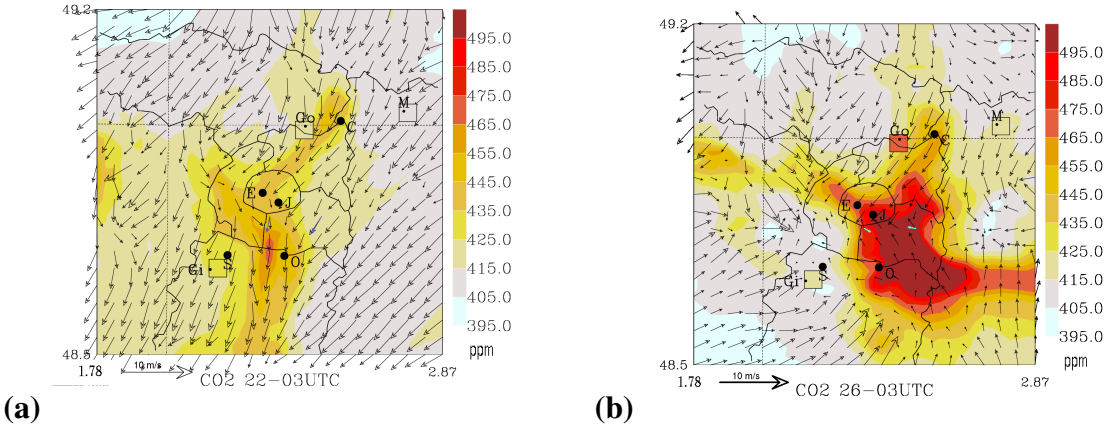

Fig. 15. Horizontal cross sections of CO_2 mixing ratio (in ppm) and predicted wind arrows (in m s^{-1}) near the ground for **(a)** March 22 at 03:00 UTC, **(b)** 26 March at 03:00 UTC.

in turquoise arrows) could explain it. The situation differs from the previous days when the well-established northeasterly winds dilute the pollutant, smoothing the CO_2 increments and inducing the maximum mixing ratio values of the measurement stations at GIF site (Fig. 14a). During the first 4 days, errors on the predicted winds are small as well as on CO_2. Table 6 presents mean CO_2 mixing ratios along a rural-urban transect during the period 13:00–17:00 UTC for the 6 days with non-negligible increments. These differences are fairly well represented by the model. This demonstrates the possibility to apply inversion during daytime on urban and suburban area for ground and altitude stations.

Rural–urban contrasts on CO_2 are stronger during the night, as shown in Table 6 for the period 00:00–06:00 h. Note that unfortunately EIF should not be considered here as it is located above the UBL. Therefore, there is no dense urban station available here to compute urban–suburban increments. The increments are fairly well reproduced by the model, especially when the flux is well established like during the first 4 days, which limited the horizontal transport

Table 6. Mean CO_2 mixing ratios (in ppm) for the 2 periods 13:00–17:00 UTC and 00:00–06:00 UTC, observed and predicted for the 5 sites TRN, GIF, EIF, GON and MON.

13:00 UTC–17:00 UTC					
	TRN	GIF	EIF	GON	MON
OBS	396	401	408	403	401
REF	396	400	403	403	400
RUR	396	402	405	406	402
00:00 UTC–06:00 UTC					
	TRN	GIF	EIF	GON	MON
OBS	408	430	404	446	414
REF	406	436	404	434	411
RUR	406	438	404	434	411

errors (Fig. 15a). The complex wind circulation on 26 March at 03:00 UTC, corresponding to the maximum UHI of the period (Fig. 5), involves a stronger variability on CO_2. It is mostly represented by the model, but the complex mesoscale circulation, associated to the UHI, is a source of transport errors, as illustrated by the observed wind arrows (Fig. 13b). Applying inversion in the nocturnal UBL is more appropriate on urban than rural sites due to the vertical mixing, caught by the urban parameterisation, but it must rely on a significant period of well-established flux to limit horizontal transport errors.

6 Conclusions

In order to better understand the effects that mesoscale transport has on atmospheric CO_2 distributions in urban and suburban areas, the mesoscale atmospheric model Meso-NH coupled with the Town Energy balance (TEB) urban canopy scheme and with the Interactions between Soil, Biosphere and Atmosphere CO_2-reactive (ISBA-A-gs) surface scheme was run for the period from 21 March to 26 March in 2011 covering the campaign of CO_2-MEGAPARIS project. The validation of forward modelling of CO_2 transport is essential to validate the system and also to show its potential in the context of inverse modelling when using high-frequency CO_2 mixing ratio data. For rural stations, it is well known that only afternoon values of CO_2 mixing ratio are well appropriate for estimating carbon sources/sinks on land, and preferentially for data sampled several hundred metres above ground as they are representative of regional fluxes and also as they can be represented substantially more robustly in atmospheric models (Geels et al., 2007). In this context, the objective of our study was to assess the capability of the modelling system to be used on urban and suburban area in inverse studies.

During daytime, the model captures well the onset time of the BLH thickening in the morning as well as the growth rates at all the different sites. Indeed, the timing of CO_2 mixing ratio spikes at the Eiffel Tower, occurring when the BLH reaches the measurement height, is remarkably well reproduced corresponding to the growing phase of the ABL. Also, at the ground stations, minimum predicted and measured mixing ratios are in agreement, with significant horizontal increments linked to urban–rural contrasts on BLH. This suggests to apply inversion during daytime in the urban and suburban area not only in the afternoon but also including the morning, and not only for tower sites but also for ground stations.

During nighttime in the urban area, the difficulty for the models to reproduce the vertical transport correctly is not as strong as for the rural area due to the NBL mixing avoiding the stable boundary layer conditions. However, observed nocturnal CO_2 mixing ratios show a high spatio-temporal variability on the suburban area with strong maxima at rush hours (at the beginning and at the end of the night) in the contracted ABL, which is challenging to simulate. Meso-NH succeeds in reproducing the timing of the nocturnal CO_2 mixing ratio at urban and suburban sites. Discrepancies on nocturnal CO_2 mixing ratios are consecutive to vertical transport errors, with a mean negative bias of 5 m on the BLH over SIRTA during nighttime, and also maybe to horizontal transport errors and to the spatio-temporal inaccuracy of anthropogenic emissions over the city and the airports. The urban parameterisation scheme TEB proved crucial in reproducing the UHI, the urban–rural contrasts on BLH and the CO_2 diurnal cycle. The limited duration comparison between CO_2 observation and modelling does not allow generalisation of the model performance, but the daily runs over 1 yr provide a very good evaluation of the BLH in the suburban area, which gives confidence in the modelling database. This 1 yr of Meso-NH forward modelling can now be used for inverse methods based on the CO_2-MEGAPARIS measurement network. The study also demonstrates the potential of the CO_2-MEGAPARIS stations to be used for inverse methods as the stations offer an adequate and comprehensive database to quantify surface fluxes and are devoted to monitor long-term measurements of CO_2. However, additional CO_2 stations, especially ground stations in denser parts of the city, would be beneficial.

Supplementary material related to this article is available online at: http://www.atmos-chem-phys.net/13/4941/2013/acp-13-4941-2013-supplement.pdf.

Acknowledgements. This work has been partially supported by the CO_2-MEGAPARIS project funded by the Agence Nationale de Recherche. The authors wish to thank all those who worked to collect the data in the field, especially M. Schmidt and M. Lopez, who provided measurements at TRN and GIF. Also thanks to C. Treguer and M. Kebe for their contribution to the scores computation. We would like to thank two anonymous reviewers for their helpful comments.

Edited by: R. Cohen

The publication of this article is financed by CNRS-INSU.

References

Ahmadov, R., Gerbig, C., Kretschmer, R., Körner, S., Rödenbeck, C., Bousquet, P., and Ramonet, M.: Comparing high resolution WRF-VPRM simulations and two global CO_2 transport models with coastal tower measurements of CO_2, Biogeosciences, 6, 807–817, doi:10.5194/bg-6-807-2009, 2009.

Angevine, W. M., White, A., Senff, C. J., Trainer, M., Banta, R. M., and Ayoub, M. A.: Urban-rural contrasts in mixing height and cloudiness over Nashville in 1999, J. Geophys. Res., 108, 4092–4099, 2003.

Bougeault, P. and Lacarrere, P.: Parameterization of orography-induced turbulence in a meso-beta scale model, Mon. Weather Rev., 117, 1870–1888, 1989.

Calvet, J.-C., Noilhan, J., Roujean, J.-L., Bessemoulin, P., Cabelguenne, M., Olioso, A., and Wigneron, J.-P.: An interactive vegetation SVAT model tested against data from six contrasting sites, Agric. Forest Meteorol., 92, 73–95, doi:10.1016/S0168-1923(98)00091-4, 1998.

Cuxart, J., Bougeault, P., and Redelsperger, J.-L.: a multiscale turbulence scheme apt for LES and mesoscale modelling, Q. J. Roy. Meteor. Soc., 126, 1–30, 2000.

De Arellano, J. V.-G., Gioli, B., Miglietta, F., Jonker, H. J. J., Baltink, H. K., Hutjes, R. W. A., and Holtslag, A. A. M.: Entrainment process of carbon dioxide in the atmospheric boundary layer, J. Geophys. Res., 109, D18110, doi:10.1029/2004JD004725, 2004.

Dolman, A., Noilhan, J., Durand, P., Sarrat, C., Brut, A., Butet, A., Jarosz, N., Brunet, Y., Loustau, D., Lamaud, E., Tolk, L., Ronda, R., Miglietta, F., Gioli, B., Magliulo, E., Esposito, M., Gerbig, C., Korner, S., Galdemard, P., Ramonet, M., Ciais, P., Neininger, B., Hutjes, R., Elbers, J., Warnecke, T., Landa, G., Sanz, M., Scholz, Y., and Facon, G.: CERES, the CarboEurope Regional Experiment Strategy in Les Landes, south-west France, May–June 2005, B. Am. Meteorol. Soc., 87, 1367–1379, 2006.

Engelen, R. J., S. Serrar and F. Chevallier, 2009: Four-dimensional data assimilation of atmospheric CO_2 using AIRS observations, J. Geophys. Res., doi:10.1029/2008JD010739.

Enting, I. G.: Inverse problems in atmospheric constituent studies: III Estimating errors in surface sources, Inverse Probl., 9, 649–665, 1993.

Forster, P., Ramaswamy, V., Artaxo, P., Berntsen, T., Betts, R., Fahey, D. W., Haywood, J., Lean, J., Lowe, D., Myhre, G., Ngang, J., Prinn, R., Raga, G., Schulz, M., and Dorland, R. V.: Changes in atmospheric constituents and in radiative forcing, in: Climate Change 2007: The Physical Science Basis. Contribution of Working Group I to the Fourth Assessment Report of the Intergovernmental Panel on Climate Change, Cambridge University Press, Cambridge, UK and New York, NY, USA, 2007.

Geels, C., Gloor, M., Ciais, P., Bousquet, P., Peylin, P., Vermeulen, A. T., Dargaville, R., Aalto, T., Brandt, J., Christensen, J. H., Frohn, L. M., Haszpra, L., Karstens, U., Rödenbeck, C., Ramonet, M., Carboni, G., and Santaguida, R.: Comparing atmospheric transport models for future regional inversions over Europe – Part 1: mapping the atmospheric CO_2 signals, Atmos. Chem. Phys., 7, 3461–3479, doi:10.5194/acp-7-3461-2007, 2007.

Gerbig, C., Körner, S., and Lin, J. C.: Vertical mixing in atmospheric tracer transport models: error characterization and propagation, Atmos. Chem. Phys., 8, 591–602, doi:10.5194/acp-8-591-2008, 2008.

Gibert, F., Schmidt, M., Cuesta, J., Ciais, P., Ramonet, M., Xueref, I., Larmanonou, E., and Flamant, P. H.: Retrieval of average CO_2 fluxes by combining in situ CO_2 measurements and backscatter lidar information. J. Geophys. Res., 112, D10301, doi:10.1029/2006JD008190, 2007.

Gurney, K. R., Law, R. M., Denning, A. S., Rayner, P. J., Baker, D., Bousquet, P., Bruhwiler, L., Chen, Y. H., Cials, P., Fan, S., Fung, I. Y., Gloor, M., Heimann, M., Higuchi, K., John, J., Maki, T., Maksyutov, S., Masarie, K., Peylin, P., Prather, M., Pak, B. C., Randerson, J., Sarmiento, J., Taguchi, S., Takahashi, T., and Yuen, C. W.: Towards robust regional estimates of CO_2 Sources and Sinks Using Atmospheric Transport Models, Nature, 415, 626–630, 2002.

Gurney, K. R., Razlivanov, I., Song, Y. Zhou, Y., Benes, B., and Abdul-Massih, M.: Quantification of fossil fuel CO_2 at the building/street scale for a large US city, Environ. Sci. Technol., 46, 12194–12202 doi:10.1021/es3011282, 2012.

Hamdi, R. and Masson, V.: Inclusion of a drag approach in the town energy balance (TEB) scheme: offline 1-D validation in a street canyon, J. Appl. Meteorol. Clim., 47, 2627–2644, 2008.

Hidalgo, J., Masson, V., and Pigeon, G.: Urban-breeze circulation during the CAPITOUL experiment: numerical simulations, Meteorol. Atmos. Phys., 102, 243–262, 2008.

Kretschmer, R., Gerbig, C., Karstens, U., and Koch, F.-T.: Error characterization of CO_2 vertical mixing in the atmospheric transport model WRF-VPRM, Atmos. Chem. Phys., 12, 2441–2458, doi:10.5194/acp-12-2441-2012, 2012.

Kort, E. A., Frankenberg, C., Miller, C. E., and Oda, T.: Space-based Observations of Megacity Carbon Dioxide, Geophys. Res. Lett., doi:10.1029/2012GL052738, 2012.

Lafore, J. P., Stein, J., Asencio, N., Bougeault, P., Ducrocq, V., Duron, J., Fischer, C., Héreil, P., Mascart, P., Masson, V., Pinty, J. P., Redelsperger, J. L., Richard, E., and Vilá-Guerau de Arellano, J.: The Meso-NH Atmospheric Simulation System. Part I: adiabatic formulation and control simulations, Ann. Geophys., 16, 90–109, doi:10.1007/s00585-997-0090-6, 1998.

Lauvaux, T., Uliasz, M., Sarrat, C., Chevallier, F., Bousquet, P., Lac, C., Davis, K. J., Ciais, P., Denning, A. S., and Rayner, P. J.: Mesoscale inversion: first results from the CERES campaign with synthetic data, Atmos. Chem. Phys., 8, 3459–3471, doi:10.5194/acp-8-3459-2008, 2008.

Lauvaux, T., Pannekoucke, O., Sarrat, C., Chevallier, F., Ciais, P., Noilhan, J., and Rayner, P. J.: Structure of the transport uncertainty in mesoscale inversions of CO_2 sources and sinks using ensemble model simulations, Biogeosciences, 6, 1089–1102, doi:10.5194/bg-6-1089-2009, 2009.

Lee, S.-H., Kim, S.-W., Angevine, W. M., Bianco, L., McKeen, S. A., Senff, C. J., Trainer, M., Tucker, S. C., and Zamora, R. J.: Evaluation of urban surface parameterizations in the WRF model using measurements during the Texas Air Quality Study 2006 field campaign, Atmos. Chem. Phys., 11, 2127–2143, doi:10.5194/acp-11-2127-2011, 2011.

Lemonsu, A., Pigeon, G., Masson, V., and Moppert, C.: Sea-town interactions over Marseille: 3D urban boundary layer and thermodynamic fields near the surface, Theor. Appl. Climatol., 84, 171–178, 2006.

Lemonsu, A., Masson, V., Shashua-Bar, L., Erell, E., and Pearlmutter, D.: Inclusion of vegetation in the Town Energy Balance

model for modeling urban green areas, Geosci. Model Dev., 5, 1377–1393, doi:10.5194/gmd-5-1377-2012, 2012.

Lin, J. C. and Gerbig, C.: Accounting for the effect of transport errors on tracer inversions, Geophys. Res. Lett., 32, L01802, doi:10.1029/2004GL021127, 2005.

Masson, V.: A physically-based scheme for the urban energy budget in atmospheric models, Bound.-Layer Meteorol, 1994, 357–397, 2000.

Masson, V.: Urban surface modeling and the meso-scale impact of cities, Theor. Appl. Climatol., 84, 35–45, 2006.

Masson, V. and Seity, Y.: Including atmospheric layers in vegetation and urban offline surface schemes, J. Appl. Meteorol. Clim., 48, 1377–1397, 2009.

Masson, V., Champeaux, J.-L., Chauvin, C., Meriguet, C., and Lacaze, R.: A global database of land surface parameters at 1 km resolution for use in meteorological and climate models, J. Climate, 16, 1261–1282, 2003.

Masson, V., Moigne, P. L., Martin, E., Faroux, S., Alias, A., Alkama, R., Belamari, S., Barbu, A., Boone, A., Bouyssel, F., Brousseau, P., Brun, E., Calvet, J.-C., Carrer, D., Decharme, B., Delire, C., Donier, S., Essaouini, K., Gibelin, A.-L., Giordani, H., Habets, F., Jidane, M., Kerdraon, G., Kourzeneva, E., Lafaysse, M., Lafont, S., Brossier, C. L., Lemonsu, A., Mahfouf, J.-F., Marguinaud, P., Mokhtari, M., Morin, S., Pigeon, G., Salgado, R., Seity, Y., Taillefer, F., Tanguy, G., Tulet, P., Vincendon, B., Vionnet, V., and Voldoire, A.: The SURFEXv7.2 land and ocean surface platform for coupled or offline simulation of Earth surface variables and fluxes, Geosci. Model Dev. Discuss., 5, 3771–3851, doi:10.5194/gmdd-5-3771-2012, 2012.

McGrath-Spangler, E. and Denning, A.: Impact of entrainment from overshooting thermals on land-atmosphere interactions during summer 1999, Tellus, 62, 441–454, doi:10.1111/j.1600-0889.2010.00482.x, 2010.

Noilhan, J. and Planton, S.: A simple parameterization of land surface processes for meteorological models, Mon. Weather Rev., 117, 536–549, 1989.

Noilhan, J., Donier, S., Lacarrère, P., Sarrat, C., and LeMoigne, P.: Regional scale evaluation of a land surface scheme from atmospheric boundary layer observations, J. Geophys. Res., 116, D01104, doi:10.1029/2010JD014671, 2011.

Pal, S., Behrendt, A. and Wulfmeyer, V.: Elastic-backscatter-lidar-based characterization of the convective boundary layer and investigation of related statistics, Ann. Geophys., 28, 825–847, doi:10.5194/angeo-28-825-2010, 2010.

Pal, S., Xueref-Remy, I., Ammoura, L., Chazette, P., Gibert, F., Royer, P., Dieudonné, E., Dupont, J.-C., Haeffelin, M., Lac, C., Lopez, M., Morille, Y., and Ravetta, F.: Spatio-temporal variability of the atmospheric boundary layer depth over Paris agglomeration: an assessment of the impact of urban heat island intensity, Atmos. Environ., 63, 261–275, doi:10.1016/j.atmosenv.2012.09.046, 2012.

Pérez-Landa, G., Ciais, P., Gangoiti, G., Palau, J. L., Carrara, A., Gioli, B., Miglietta, F., Schumacher, M., Millán, M. M., and Sanz, M. J.: Mesoscale circulations over complex terrain in the Valencia coastal region, Spain – Part 2: Modeling CO_2 transport using idealized surface fluxes, Atmos. Chem. Phys., 7, 1851–1868, doi:10.5194/acp-7-1851-2007, 2007.

Pergaud, J., Masson, V., Malardel, S., and Couvreux, F.: A parameterization of dry thermals and shallow cumuli for mesoscale numerical weather prediction, Bound.-Layer Meteor., 132, 83–106, 2009.

Pinty, J. and Jabouille, P.: A mixed-phased cloud parameterizations for use in a mesoscale non-hydrostatic model: simulations of a squall line and of orographic precipitation, in: Conf. on Cloud Physics, 217–220, Amer. Meteor. Soc., Everett, WA, USA, 1998.

Rödenbeck, C., Houweling, S., Gloor, M., and Heimann, M.: CO_2 flux history 1982–2001 inferred from atmospheric data using a global inversion of atmospheric transport, Atmos. Chem. Phys., 3, 1919–1964, doi:10.5194/acp-3-1919-2003, 2003.

Sarrat, C., Noilhan, J., Dolman, A. J., Gerbig, C., Ahmadov, R., Tolk, L. F., Meesters, A. G. C. A., Hutjes, R. W. A., Ter Maat, H. W., Pérez-Landa, G., and Donier, S.: Atmospheric CO_2 modeling at the regional scale: an intercomparison of 5 meso-scale atmospheric models, Biogeosciences, 4, 1115–1126, doi:10.5194/bg-4-1115-2007, 2007a.

Sarrat, C., Noilhan, J., Lacarrère, P., Donier, S., Lac, C., Calvet, J.-C., Dolman, H., Gerbig, C., Neininger, B., Ciais, P., Paris, J. D., Boumard, F., Ramonet, M., and Butet, A.: Atmospheric CO_2 modeling at the regional scale: application to the CarboEurope regional experiment, J. Geophys. Res., 112, D12105, doi:10.1029/2006JD008107, 2007b.

Sarrat, C., Noilhan, J., Lacarrère, P., Masson, V., Ceschia, E., Ciais, P., Dolman, A., Elbers, J., Gerbig, C., and Jarosz, N.: CO_2 budgeting at the regional scale using a Lagrangian experimental strategy and meso-scale modeling, Biogeosciences, 6, 113–127, doi:10.5194/bg-6-113-2009, 2009.

Seibert, P., Beyrich, F., Gryning, S. E., Joffre, S., Rasmussen, A., and Tercier, P.: Review and intercomparison of operational methods for the determination of the mixing height, Atmos. Environ., 34, 1001–1027, 2000.

Seity, Y., Brousseau, P., Malardel, S., Hello, G., Bénard, P., Bouttier, F., Lac, C., and Masson, V.: The AROME-France Convective-Scale Operational Model, Mon. Weather Rev., 139, 976–991, 2010.

Sorensen, J. H., Rasmussen A. and Svensmark H. : Forecast of Atmospheric Boundary Layer Height Utilised for ETEX Real-time Dispersion Modelling, Phys. Chem. Earth, 21, 435–439, 1996.

Steeneveld, G., Mauritsen, T., Bruijn, E. D., de Arellano, J. V.-G., Svensson, G., and Holtslag, A.: Evaluation of limited-area models for the representation of the diurnal cycle and contrasting nights in CASES-99, J. Appl. Meteor. Clim., 47, 869–887, doi:10.1175/2007JAMC1702.1, 2008.

Strong, C., Swertka, C., Bowling, D. R., Stevens, B. B., and Ehleringer, J. R.: Urban carbon dioxide cycles within the Salt Lake Valley: a multiple box model validated by observations, J. Geophys. Res.-Atmos., 116, D15307, 2011.

Takahashi, T., Feely, R. A., Weiss, R. F., Wanninkhof, R. H., Chipman, D. W., Sutherland, S. C., and Takahashi, T. T.: Global air-sea flux of CO_2: An estimate based on measurements of sea air CO_2 difference, Proc. Natl. Acad. Sci. USA, 94, 8292–8299, doi:10.1073/pnas.94.16.8292, 1997.

Vautard, R., Menut, L., Beekmann, M., Chazette, P., Flamant, P. H., Gombert, D., Guedalia, D., Kley, D., Lefebvre, M. P., Martin, D., Megie, G., Perros, P., and Toupance, G.: A synthesis of the air pollution over the paris region (ESQUIF) field campaign, J. Geophys. Res., 108, 8558, doi:10.1029/2003JD003380, 2003.

Xueref-Remy, I., Pal, S., Lopez, M., Schmidt, M., Dieudonné, E., Vuillemin, C., Darding, M., and Wastine, B.: Atmospheric inves-

tigation of the role of the different emission sectors in the total CO_2 emission plume from the Paris megacity, Geophys. Res. Abstr., 14, EGU2012–13419, 2012.